International Journal of Impact Engineering 166 (2022) 104238

Contents lists available at ScienceDirect

International Journal of Impact Engineering

journal homepage: www.elsevier.com/locate/ijimpeng

The role of granular buoyant force of projectile in determining the penetration depth

Hyeong Seok Koh [a], Da Yeon Shin [b], Gil Ho Yoon [*,a]

[a] School of Mechanical Engineering, Hanyang University, Seoul, South Korea
[b] School of Convergence Defense, Hanyang University, Seoul, South Korea

ARTICLE INFO

Keywords:
Granular medium
Penetration depth
Initial penetration depth
Stationary penetration depth
Buoyancy force
Free-fall projectile

ABSTRACT

This research develops a new formulation for final penetration depth of projectile on granular material. Although several relevant researches exist to estimate final penetration depths of blunt projectiles, estimation of final penetration depth of sharp projectiles is still difficult. Direct application of the formulation of blunt projectile cannot be applicable for sharp projectile. It is possible to employ heuristic and empirical formulations to predict the penetration depth of projectiles. Through several experimental studies, this research, however, finds out that buoyant force of sharp projectiles can be included in the existing formula for the final penetration depth of blunt projectiles. In order to verify the hypothesis, first of all several experiments with cylinder and ball were carried out to validate the existing theory. After sharp projectiles are experimented, the effect of the buoyant force is formulated as initial penetration depth. By adding this initial penetration depth determined by balancing between the buoyant force and weight, it is possible to adjust the existing formula for sharp projectiles. To show the validity of the present formulation, several cone shape projectiles are modeled and tested.

1. Introduction

This research develops a formulation for the final penetration depth of falling projectile onto a granular material. Estimation of the final penetration depth of a blunt (or flat) projectile has been actively studied for craters formed by impacts or explosions. However, the estimation cannot be applicable to random shape projectiles. To our best knowledge, the existing formulations are only applicable to blunt (or flat) projectiles. The direct applications of the formulations are still erroneous for random shape projectiles especially projectile with sharp nose tip (or sharp projectile). Indeed, it is only possible to employ a heuristic formulation to predict the penetration depth of the sharp projectile. After experimental and theoretical studies, this research presents a new modification that can be applied to sharp projectile considering the buoyant force.

Several relevant researches predicting penetration depths of ball and cylindrical projectiles exist [1–10]. According to impact velocity, the different physical phenomena are observed. Depending on the range of velocity, impact testing can be classified as low-velocity impact, high-velocity impact, ballistic impact and hypervelocity impact in [11]. In the hypervelocity impact, projectiles often break above a certain velocity limit [12]. In the present study, the low-velocity impact or the free-fall drop test is considered. In [1], balls are dropped into granular media in order to form a crater and investigate diameters and depths of craters. The formula of diameter and depth with respect to ball density, ball diameter and drop height were presented. In [2], the improved penetration depth of various spheres dropped into granular media is defined by the characteristics of the ball. In [3], the penetration depths of cylindrical projectiles are investigated. The role of the shape of the projectile is experimentally investigated. In [8], the diameters and depths of impact craters formed by dropping a steel ball into glass beads are investigated and it is revealed that they are proportional to the 1/3 power of energy of the projectile. This relationship is important as it shows the quantitative relationship between the penetration depth and the energy that can be used to derive the penetration depths of various projectiles and quantitatively verify the accuracy of relevant research. In [9], high speed impact formulating jet of fine sand is observed. In [10], the diameter of a crater by a small steel ball is experimentally observed. Functional dependence of the crater diameter on the kinetic energy is observed too. In addition, research with other shape projectiles exist [3, 13–15]. In [3], the penetration depths of cylindrical projectiles dropped into granular medium is tested. In [13], different nose shapes and masses

* Corresponding author.
E-mail address: ghy@hanyang.ac.kr (G.H. Yoon).

https://doi.org/10.1016/j.ijimpeng.2022.104238
Received 14 September 2021; Received in revised form 4 April 2022; Accepted 7 April 2022
Available online 12 April 2022

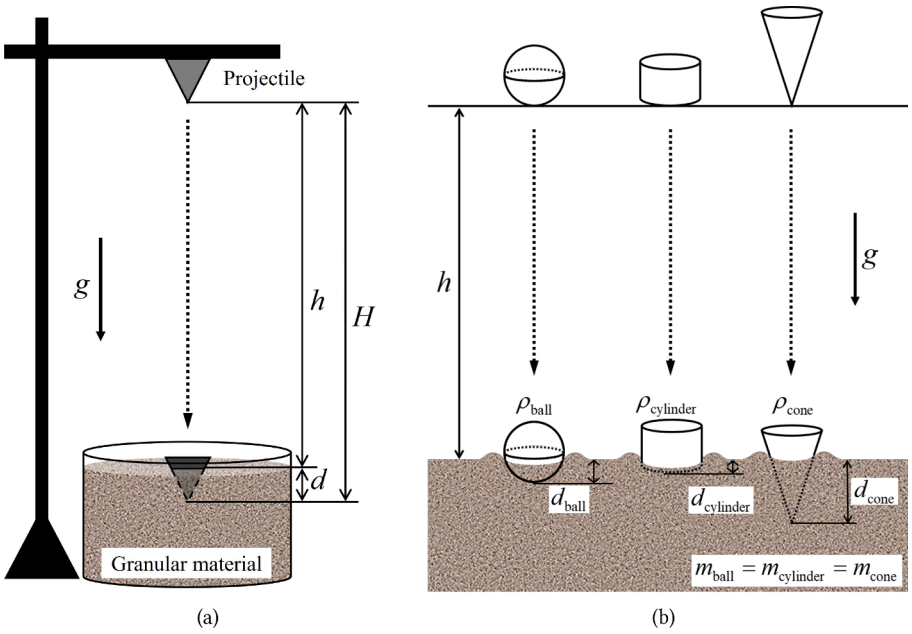

Fig. 1. The penetration depth of spherical, cylindrical and conical projectile falling. (a) The experimental setup and the definitions of the parameters and (b) the differences of the penetration depth due to the different shapes.

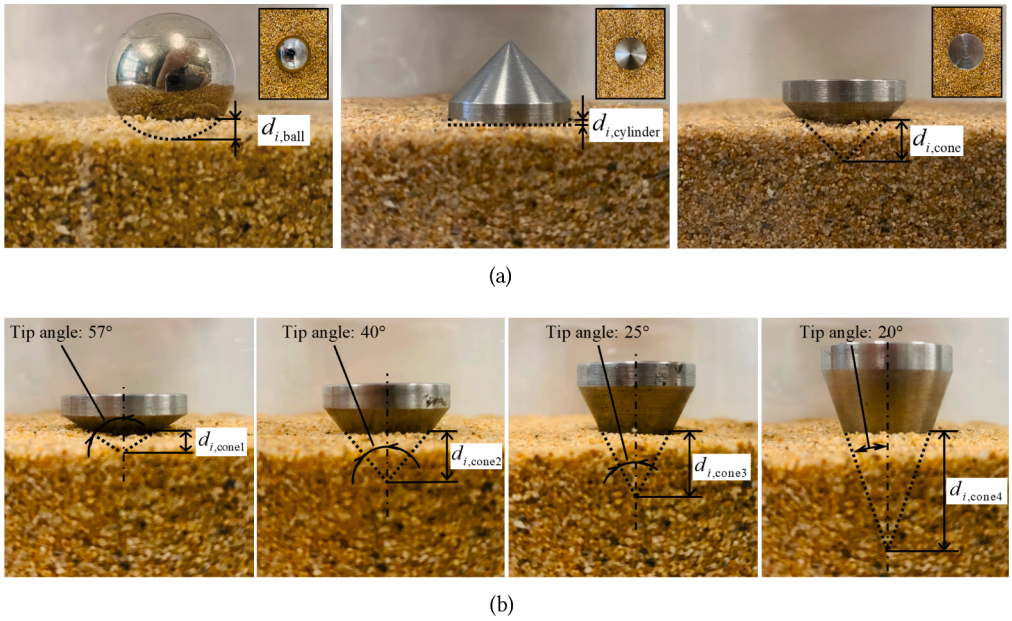

Fig. 2. (a) Morphology effect (Sharpness of projectile) on stationary penetration depth (Equivalent cylinder (Flipped cone): Mass $m_{p,cylinder}$= 32 g, Diameter $D_{p,cylinder}$= 25 mm, Equivalent height $L_{p,cylinder}$= 5.2 mm, $d_{i,cylinder}$ = 0.8 mm (The flipped cone is used for the cylinder experiment as the stationary penetration depth of a cylinder with 32 g mass can be same as that of the flipped cone with 32 g mass), Ball: Mass $m_{p,ball}$= 32 g, Diameter $D_{p,ball}$= 20 mm, $d_{i,ball}$ = 1 mm, Cone: Mass $m_{p,cone}$= 32 g, Diameter $D_{p,cone}$= 25 mm, Height $L_{p,cone}$= 15.5 mm, $d_{i,cone}$ = 6.5 mm ($m_{p,cylinder}$= $m_{p,cone}$= 32 g)) and (b) the penetration depths for the various cones (Mass: [25g 37g 50g 63g], Tip angles: [57 °, 40 °, 25 °, 20 °] from the left to the right, Heights: [8 mm, 15.5 mm, 25 mm, 36 mm]+ 4 mm (the height of the upper cylinder) from the left to the right): d_i= 3.8 mm, 9.05 mm, 12.5 mm and 18.2 mm from the left to the right.

of projectiles were fired into sand. It is observed that the heavier the mass of the projectile, the larger influence on the amount of absorbed energy. In [14], the effect of the drag force on projectiles with circular cross sections is studied. In [15], the internal flow fields in sand due to long-rod projectiles were measured and studied.

Several relevant researches regarding buoyancy force exist too [5–7, 16–22]. In [6], segregation of granular mixtures is separated through the buoyancy force. In [7], the sinking depths of balls into granular materials are measured and the geometric effect is studied. This research provides an insight regarding the sinking depth due to the buoyancy force. In [16], the internal force chains of sand are studied. In [5], the time dependency of wooden spheres penetrating into glass beads is studied. In [17], the penetration depth of a sphere projectile into a granular medium is linearly dependent on the impact momentum. In addition, the research shows that this behavior can be explained in terms of yield stress and an effective viscosity of the granular medium. In [18], the effect of projectile mass is studied. It is found that a falling object suspended in fluid reaches a terminal velocity when its weight and the drag force are balanced. When an object is heavier than a critical mass, the object reaches a terminal velocity that means an endless penetration. In [19], a unified description of low-speed impact is studied. In [20], molecular dynamics simulations and experiments are carried out to study the penetration of a two-dimensional granular media. In [21], response of a granular system to an impact was studied. In [22], flow rate of granular material is experimentally controlled by the exit velocity imposed on the particles.

By following the results of the relevant research [3,7], this research modifies the penetration depth formulation of sharp projectiles by

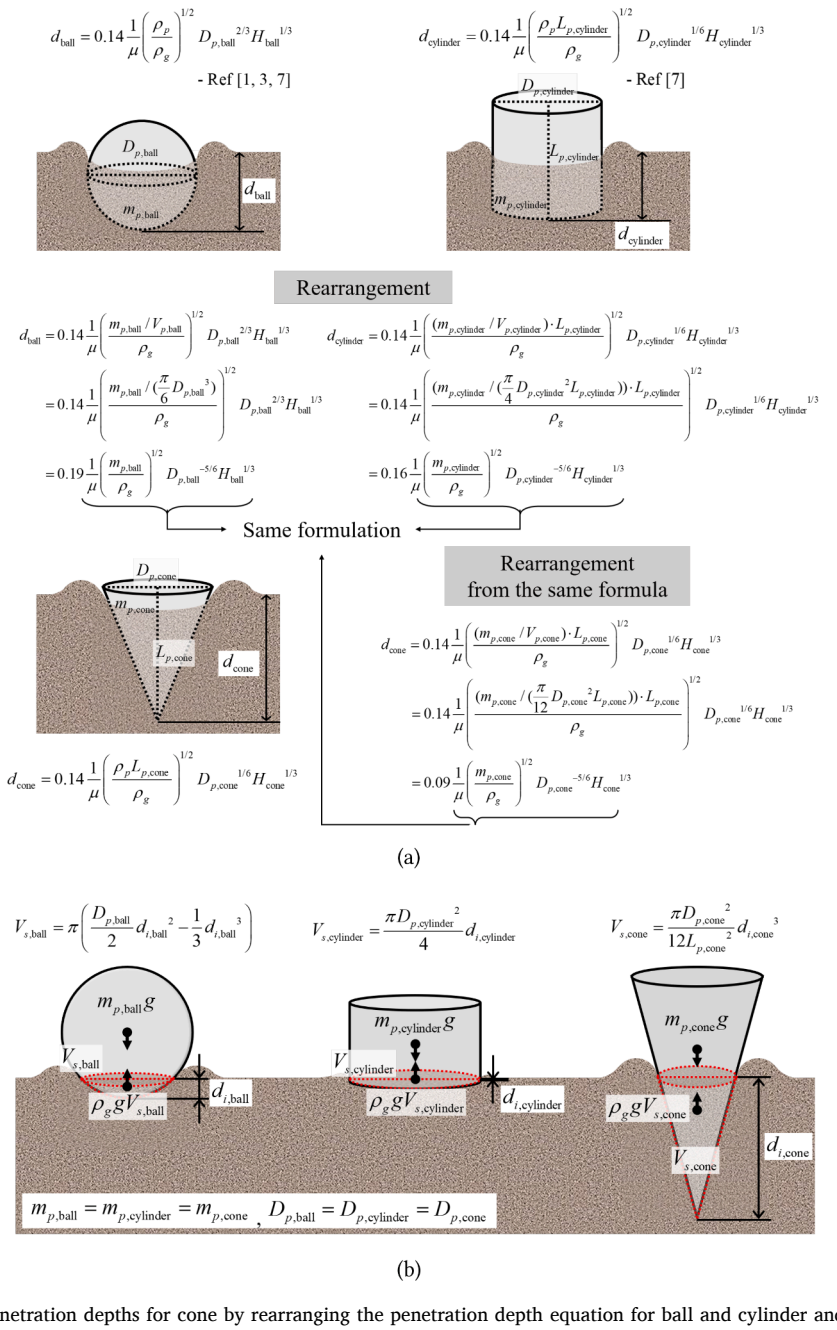

Fig. 3. (a) Estimations of the penetration depths for cone by rearranging the penetration depth equation for ball and cylinder and (b) the stationary penetration depth and the buoyancy.

subtracting the initial penetration depth due to the buoyancy force. Experimentally and theoretically, it is known that the penetration depth of blunt projectiles can be estimated. Blunt projectile refers to projectiles without sharp corner where contact with granular material [13]. For example, Fig. 1 shows the schematic diagram. With the same mass, the penetration depths of the cylinder and sphere without sharp corner are similar. The effects of the geometries such as density, radius and falling height are well studied [1,2,8]; the penetration depth is defined by d as shown in Fig. 1(b). However, the sharp projectile, here a cone shaped projectile, shows a larger penetration depth even with the same mass. This phenomenon, which is considered unpredictable, can be observed in everyday life. For example, Fig. 2(a) shows the penetration depths of the various objects including cylinder, sphere and cone shaped projectiles with the same mass. As shown, the initial penetration depths of the cylinder and the sphere are different but can be neglected compared with the falling penetration depths. The cone shaped sharp projectile however shows a large initial penetration depth which can not be neglected. In addition, Fig. 2(b) shows the penetration depths of the various cones. These initial penetration depths are determined by the balance between the buoyancy force and the weight of the projectile. In the present study, these initial penetration depths are included in order to improve the predictions of the penetration depth of sharp objects. To achieve this purpose, the present study summarizes the existing formula for cylinder and sphere. After that, we modify them by considering the initial penetration depth. From experiments with the projectiles in Fig. 4, we found that by modifying the formulations with the consideration of the initial penetration depth, the estimation is improved for sharp objects. To our best knowledge, the estimation of the penetration of blunt objects can be found in [3]. However, the estimation of the penetration of sharp objects is hardly found. In the present study, we present a modification of the existing formulation predicting the penetration depth of blunt objects by subtracting the initial penetration

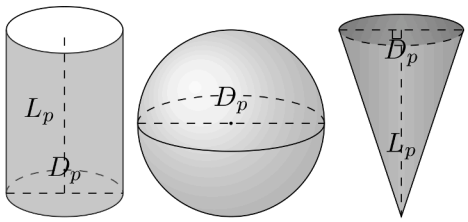

(a) (b) (c)

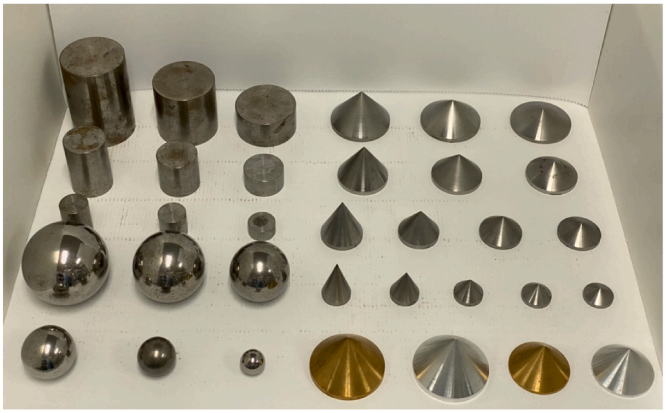

(d)

Ball (ρ_p = 7930 kg/m^3)	
D_p (mm)	m_p (g)
20	32
30	111
40	287
50	534
60	897
70	1386

Cylinder (ρ_p = 7930 kg/m^3)		
D_p (mm)	L_p (mm)	m_p (g)
25	12	46
	25	96
	37	142
38	20	177
	38	337
	57	504
60	30	665
	60	1325
	90	1989

Cone			
ρ_p (kg/m^3)	D_p (mm)	L_p (mm)	m_p (g)
7930	25	11.5	25
		17	32
		20	37
		30	50
		40	63
	38	15.6	72
		23	94
		30	111
		42	153
	48	20	138
		30	184
		40	235
	60	20	213
		30	292
		40	369
2700	48	30	60
	60	40	132
8730	48	30	187
	60	40	399

(e)

Fig. 4. Projectiles and their geometries (Without any confusion, the same symbol D_p is used to denote the diameters of the geometries). (a-c) The geometry definitions for sphere, cylinder, and cone and (d) the experimented projectiles and (e) the specification for the projectiles experimented.

depth due to the buoyancy force.

The paper is organized as follows. Section 2.1 provides some backgrounds to the penetration depth estimation of cylinder and ball. The parameters affecting the penetration depth are summarized. Section 2.2 develops the penetration depth prediction considering the buoyancy or the initial penetration depth. Section 3 summarizes the experimental results of cylinder, ball and cone that show the improvement of the prediction of projectiles. Section 4 provides the conclusions and suggestions for future research topics.

2. Prediction of the penetration depth considering the effect of buoyancy

This section provides some relevant theories and equations for the prediction of the penetration depths of several free-fall projectiles toward dry sand. In addition, a new theory predicting the effect of sharp projectiles on the penetration depth is presented. The new theory suggests that the buoyant force should be included for the sharp projectiles.

2.1. The penetration depth predictions of blunt projectiles: Ball and cylinder

Without considering the buoyancy or the initial penetration depth, the relevant empirical equations of the penetration depths of cylinder and ball were proposed in [1–3]. Through experiments and theories, the predictions are verified. However, the relevant theories and predictions are not applicable for sharp projectiles. In [3], the following theoretical equation was proposed for cylinder projectile.

$$\text{Ball (sphere)}: d_{\text{ball}} = 0.14 \frac{1}{\mu} \left(\frac{\rho_p}{\rho_g} \right)^{1/2} {D_{p,\text{ball}}}^{2/3} {H_{\text{ball}}}^{1/3} \tag{1}$$

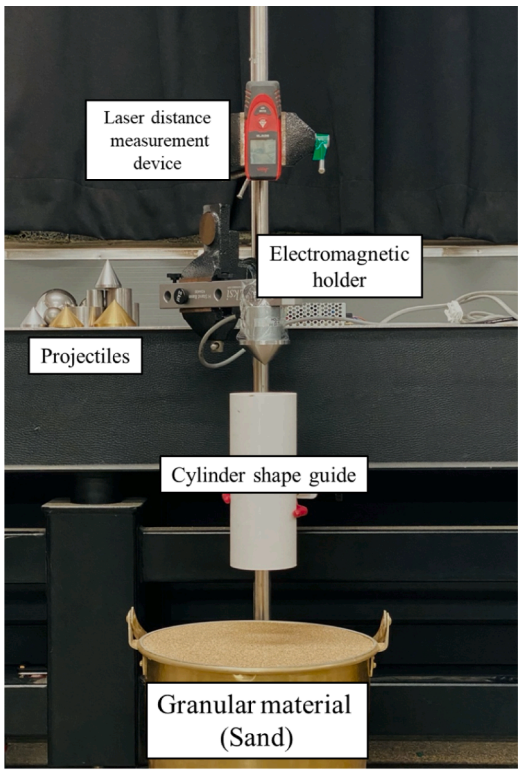

(a)

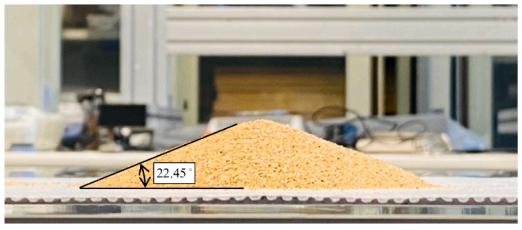

(b)

Fig. 5. (a) Experiment device: electromagnetic device dropping projectiles, cylindrical shape guide to maintain the posture of the projectile and (b) repose angle of the sand.

$$H_{\text{ball}} = h + d_{\text{ball}} \tag{2}$$

where the penetration depth of the ball projectile with diameter $D_{p,\text{ball}}$ at the dropped heigh h is denoted by d_{ball}. The density of the projectile is denoted by ρ_p. Note that the density of the granular media and the bulk density of the granular media are denoted by ρ_{gm} and $\rho_g (= \phi\rho_{gm})$, respectively when the volume fraction of grains is ϕ [23]. The conditions of sand such as size, regularity and moisture content determine the tangent of draining repose angle μ that affects the penetration depth, d_{ball}. The experimental results and the predictions with the above formulations are well matched as the initial penetration depth of cylinder can be neglected. In addition, the above penetration depth formulation is extended to the formulation for cylindrical projectile, d_{cylinder} as follows:

$$\text{Cylinder: } d_{\text{cylinder}} = 0.14\frac{1}{\mu}\left(\frac{\rho_p L_{p,\text{cylinder}}}{\rho_g}\right)^{1/2} {D_{p,\text{cylinder}}}^{1/6} {H_{\text{cylinder}}}^{1/3} \tag{3}$$

$$H_{\text{cylinder}} = h + d_{\text{cylinder}} \tag{4}$$

where the length and the diameter of the cylinder are denoted by $L_{p,\text{cylinder}}$ and $D_{p,\text{cylinder}}$, respectively. Again the conditions of sand such as size, regularity and moisture content affect the tangent of the draining repose angle value of μ. With elementary equipment, it is possible to verify the above relationships.

The present study notices that the above equations are accurate and reliable [1,2,8,10]. However, they neglect the effect of the initial depth of projectile. To our best knowledge, it is observed from an experimental point of view and it has not been explained reasonably and rigorously. The present study observes that the effect of the buoyancy force or the initial penetration depth can be a clue to improve the accuracy of the penetration depth estimation.

2.2. The new penetration depth prediction considering the buoyancy or the initial penetration depth

This research finds that the theories for penetration should be modified by considering the stationary penetration depth depending on the morphology of projectile. Although projectiles are placed smoothly on the surface of sand, the penetration depths become different even with the same mass owing to the buoyant force and the interaction with sand and projectiles. For example, Fig. 2(a) shows differences of the penetration depth of the same mass (32 g) on sand. Although the mass values of the projectiles are the same, the initial penetration depths or the stationary penetration depths are different. The initial penetration depth of the cylinder can be neglected and can be set to 0 whereas the initial penetration depths of the sharp objects are not negligible. The differences in the stationary penetration depths are due to the differences in friction between projectiles and sand (the buoyant forces of projectiles) as shown in Fig. 3(b). To our best knowledge, however, these differences have not been considered in the relevant researches as shown in Fig. 3(a) [6,7,16].

The buoyant force through sand can be realized when you walk across a beach. When you walk on sand, sand moves due to your weight and at some point, your foot is firmly supported due to the buoyant force. These physical phenomena occur for anything dropped from rest into sand. The potential energy (mgH) of an object of mass m dropped from a H distance above sand is transferred to sand. Some of these energies are dissipated inside sand due to the interaction between sand and projectile. At the same time, some of these energies are converted back to the gravitational energy to form a crater. The buoyant force is an upward force applied on an object immersed in fluid. In case of fluid, the magnitude of the buoyant force is determined to the weight of the immersed object (i.e., $mg = \rho_g g V_s, V_s$: Submerged volume). However, in case of granular media, the magnitude of the buoyant force is not directly determined but proportional to the weight of the immersed object :

$$m_p g \propto \rho_g g V_s \tag{5}$$

where the mass of the projectile is denoted by m_p. By manipulating the above Eq. (5), the submerged volumes of the ball projectile and the cylinder projectile can be obtained as follows:

$$m_{p,\text{ball}} \propto \frac{D_{p,\text{ball}}}{2} {d_{i,\text{ball}}}^2 \left(\text{assuming } D_{p,\text{ball}} \gg d_{i,\text{ball}}\right)$$
$$d_{i,\text{ball}} \propto \left[m_{p,\text{ball}} / D_{p,\text{ball}}\right]^{1/2} \tag{6}$$

$$d_{i,\text{cylinder}} \propto m_{p,\text{cylinder}} / {D_{p,\text{cylinder}}}^2 \tag{7}$$

where the submerged volumes of the ball projectile and the cylinder projectile are denoted by $V_{s,\text{ball}}$ and $V_{s,\text{cylinder}}$, respectively.

After considering the above initial penetration depths of the ball and cylinder projectiles, this research insists that the formulations predicting the penetration depths of the ball projectile and the cylinder projectile can be modified as follows:

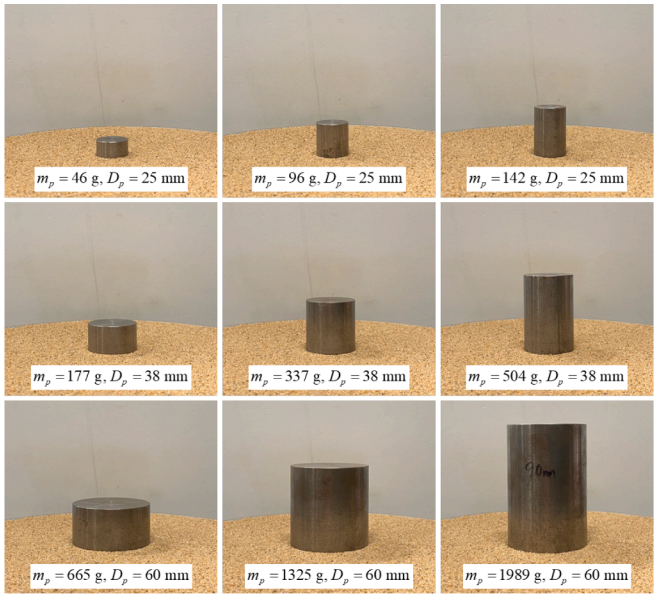

(a)

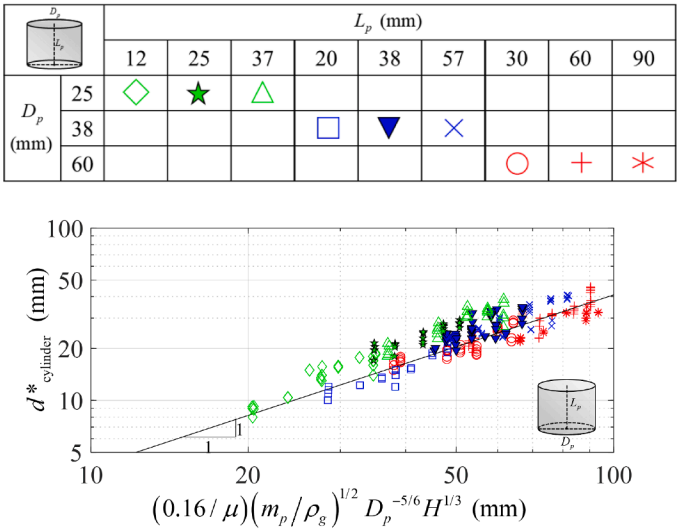

(b)

Fig. 6. Penetration depth of the cylinder projectile considering the buoyancy force. (a) The initial penetration depth distributions and (b) the modified penetration depth distributions considering the initial penetration depth (Green diamond: D_p = 25 mm, L_p=12.5 mm, Green filled star: D_p = 25 mm, L_p= 25 mm, Green upward-pointing triangle: D_p = 25 mm, L_p= 37 mm, Blue square: D_p = 38 mm, L_p=19 mm, Blue filled downward-pointing triangle: D_p = 38 mm, L_p= 38 mm, Blue x mark: D_p = 38 mm, L_p=57 mm, Red circle: D_p = 60 mm, L_p= 30 mm, Red plus mark: D_p = 60 mm, L_p= 60 mm, Red star mark: D_p = 60 mm, L_p= 90 mm). (For interpretation of the references to colour in this figure legend, the reader is referred to the web version of this article.)

$$\text{Ball: } \underbrace{d_{\text{ball}} - d_{i,\text{ball}}}_{\text{Effect of the buoyancy}} = 0.19\frac{1}{\mu}\left(\frac{m_{p,\text{ball}}}{\rho_g}\right)^{1/2} {D_{p,\text{ball}}}^{-5/6} {H_{\text{ball}}}^{1/3},\ d_{i,\text{ball}} \approx 0 \tag{8}$$

Note that the above formulas are modified by subtracting $d_{i,\text{ball}}$ and $d_{i,\text{cylinder}}$. The experimental data of the initial penetration depth of ball and cylinder projectiles presented in the next section show very small values. It should be emphasized that the above formulas without the terms associated with the buoyancy are still valid from an engineering

Cylinder:

$$\underbrace{d_{\text{cylinder}} - d_{i,\text{cylinder}}}_{\text{Effect of the buoyancy}} = 0.16\frac{1}{\mu}\left(\frac{m_{p,\text{cylinder}}}{\rho_g}\right)^{1/2} {D_{p,\text{cylinder}}}^{-5/6} {H_{\text{cylinder}}}^{1/3}, \tag{9}$$

$d_{i,\text{cylinder}} \approx 0$.

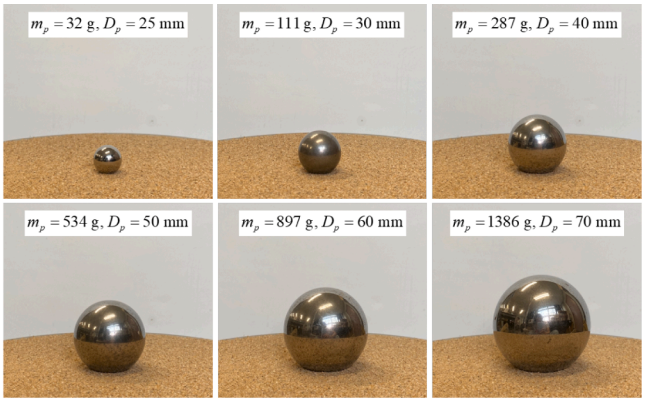

(a)

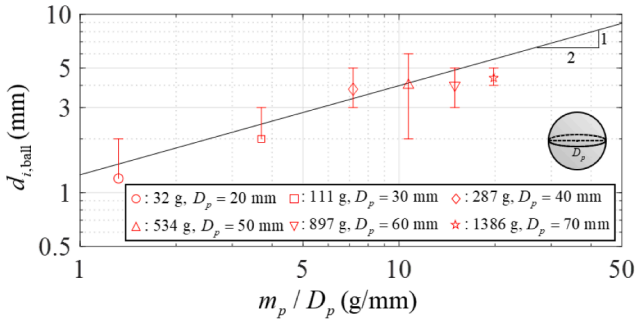

(b)

Fig. 7. Penetration experiment of ball projectiles. (a) The initial penetration depth distributions and (b) the experiment results of initial penetration depth distributions with respect to m_p/D_p (i.e. $d_{i,\mathrm{ball}} \approx (m_p/D_p)^{1/2}$).

point of view.

2.3. The penetration depth for sharp projectile: Cone

This research notices that the consideration of the buoyant force in estimating the penetration depth is important in the case of sharp projectiles as shown in Fig. 2(b) [6,7,16]. To investigate this aspect, the cone shape projectile whose sharpness can be easily controlled is considered in this research as a representative sharp projectile. The initial penetration depth due to the buoyant force can be obtained experimentally and theoretically. The same procedure in Eqs. (8) and (9) can also be applied to the estimation of the penetration depth of the cone shape projectile as illustrated in Fig. 3(a). The submerged volume of the conical projectile $V_{s,\mathrm{cone}}$ is represented with the initial penetration depth, $d_{i,\mathrm{cone}}$, as follow:

$$V_{s,\mathrm{cone}} = \frac{\pi {D_{p,\mathrm{cone}}}^2}{12 {L_{p,\mathrm{cone}}}^2} {d_{i,\mathrm{cone}}}^3. \tag{10}$$

Using the relationship between the submerged volume and the mass of the projectile, the initial penetration depth due to the buoyancy force can be expressed as following:

$$\begin{aligned} m_{p,\mathrm{cone}} g &= \rho_g g \frac{\pi {D_{p,\mathrm{cone}}}^2}{12 {L_{p,\mathrm{cone}}}^2} {d_{i,\mathrm{cone}}}^3 \\ m_{p,\mathrm{cone}} &\propto \left(\frac{D_{p,\mathrm{cone}}}{L_{p,\mathrm{cone}}}\right)^2 {d_{i,\mathrm{cone}}}^3 \\ m_{p,\mathrm{cone}} &\propto \tan^2\theta_p {d_{i,\mathrm{cone}}}^3 \end{aligned} \tag{11}$$

where the mass, diameter and the length of the cone shape projectile are denoted by $m_{p,\mathrm{cone}}$, $D_{p,\mathrm{cone}}$ and $L_{p,\mathrm{cone}}$, respectively. The tip angle of the projectile θ_p, is set to $D_{p,\mathrm{cone}}/2L_{p,\mathrm{cone}}$. Thus, the initial penetration depth of the cone shape projectile can be defined as follow:

$$d_{i,\mathrm{cone}} \propto \left[m_{p,\mathrm{cone}} \tan^{-2}\theta_p\right]^{1/3}. \tag{12}$$

The above formula implies that the initial penetration depth is proportional to one-third power of the mass, which will be validated through the experiments in the next section. And the penetration depth of the conical projectile derived from the previous formula is as following (See Fig. 3(a)):

$$\begin{aligned} d_{\mathrm{cone}} &= 0.14 \frac{1}{\mu}\left(\frac{\rho_p L_{p,\mathrm{cone}}}{\rho_g}\right)^{1/2} {D_{p,\mathrm{cone}}}^{1/6} {H_{\mathrm{cone}}}^{1/3} \\ &= 0.14 \frac{1}{\mu}\left(\frac{\left(m_{p,\mathrm{cone}}/V_{p,\mathrm{cone}}\right) L_{p,\mathrm{cone}}}{\rho_g}\right)^{1/2} {D_{p,\mathrm{cone}}}^{2/3} {H_{\mathrm{cone}}}^{1/3} \\ &= 0.14 \frac{1}{\mu}\left(\frac{m_{p,\mathrm{cone}} L_{p,\mathrm{cone}} \Big/ \left(\frac{\pi}{12} {D_{p,\mathrm{cone}}}^2 L_{p,\mathrm{cone}}\right)}{\rho_g}\right)^{1/2} {D_{p,\mathrm{cone}}}^{2/3} {H_{\mathrm{cone}}}^{1/3} \\ &= 0.09 \frac{1}{\mu}\left(\frac{m_{p,\mathrm{cone}}}{\rho_g}\right)^{1/2} {D_{p,\mathrm{cone}}}^{-5/6} {H_{\mathrm{cone}}}^{1/3} \end{aligned} \tag{13}$$

where the penetration depth of the cone shape projectile is denoted by d_{cone} and the sum of the h and the d_{cone} is denoted by H_{cone}. The above formula presents the penetration depth of cone shape projectile without considering the initial penetration depth. Considering the buoyancy force, this research presents the following formula with the initial penetration depth, $d_{i,\mathrm{cone}}$. Note that the penetration depth estimation model of the cone shape projectile is modified as fallow:

$$\underbrace{d_{\mathrm{cone}} - d_{i,\mathrm{cone}}}_{\text{Effect of buoyancy}} = d^*_{\mathrm{cone}} = 0.09 \frac{1}{\mu}\left(\frac{m_{p,\mathrm{cone}}}{\rho_g}\right)^{1/2} {D_{p,\mathrm{cone}}}^{-5/6} {H_{\mathrm{cone}}}^{1/3}. \tag{14}$$

The superscript (*) is employed to consider the initial penetration depth. The above Eq. (14) implies that for sharp projectiles the initial penetration depth can be included to find out the penetration depth of the projectile. In the next section, some experiments are carried out to verify the relationships and the associated formulas. Until this section, the shape of the projectile is denoted in the subscript of each expressions. In the next section, according to the definition in Fig. 4, the simplified symbols m_p and D_p are applied ($m_{p,\mathrm{ball}} = m_{p,\mathrm{cylinder}} = m_{p,\mathrm{cone}} = m_p$ and $D_{p,\mathrm{ball}} = D_{p,\mathrm{cylinder}} = D_{p,\mathrm{cone}} = D_p$).

3. Experimentation and verification

3.1. Experiment procedure

To investigate the effect of the initial penetration depth on the maximum penetration depth and verify the modified formulation, some experiments with cylinder, ball and cone shape projectiles are conducted in this section (Fig. 4). The projectiles are made of stainless steel, aluminum or brass to verify the effect of the buoyant force; note that it is difficult to have projectiles with the same shape and material but with different masses. An experimental device in Fig. 5 is prepared [1–5,8,10,17]. The roughly estimated diameters of sand range from 0.5 mm up to 1 mm. The measured density of granular material is 380 kg/m^3 when the measured bulk density is 1450 kg/m^3. It is interestingly found that a container should be large enough to prevent the boundary effect [4]. In this study, a cylinder shape bucket with 250 mm diameter and 300 mm depth is employed. Sand in the container is whisked lightly and tapped horizontally before the experiment as it was reported that the treatment of the surface of sand affects the results of the experiments. To adjust the sand surface without compaction, the sand surface is trimmed a few times with a straight alignment bar. The experiment is repeated several

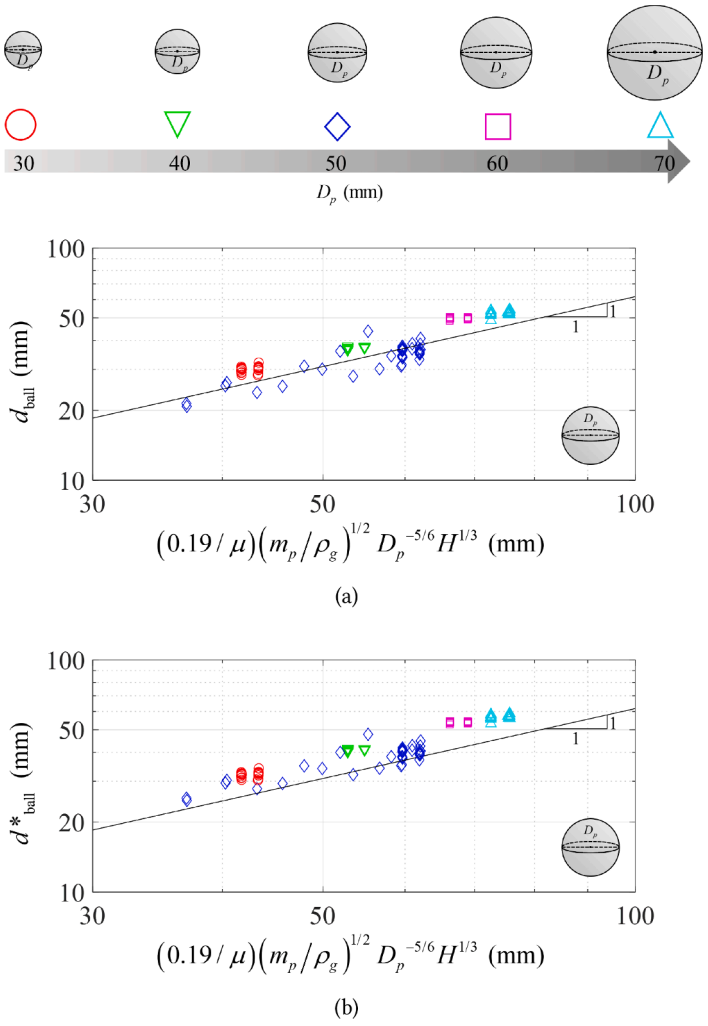

Fig. 8. Penetration depth of the ball projectile. (a) The penetration depth distributions without considering the initial penetration depth and (b) the modified penetration depth distributions considering the initial penetration depth (Red circle: $D_p = 30$ mm, Green downward-pointing triangle: $D_p = 40$ mm, Blue diamond: $D_p = 50$ mm, Magenta square: $D_p = 60$ mm, cyan upward-pointing triangle: $D_p = 70$ mm). (For interpretation of the references to colour in this figure legend, the reader is referred to the web version of this article.)

times and processed by averaging the measured penetration depths. The projectiles are dropped from 0 mm to 1000 mm range of the falling height (h). This range makes the impact velocity from 0 m/s to 4.43 m/s by ignoring the effect of air. While cylinders or balls are relatively easy to drop vertically, it is complicated to drop vertically for cone. Indeed a cylinder guider is installed. The penetration depth and the free-fall distance are measured with a laser distance measurement device. The validity of the experiment device is carried out by measuring the penetration depths and comparing the effects of geometries of the falling projectiles, i.e., cylinder and ball.

3.2. Experiment with cylinder and ball

For the first experiment, the projectiles of cylinder and ball depicted in Fig. 4 are dropped with the mentioned experimental setup. The initial penetration depths of cylinder projectiles are almost zeros as depicted in Fig. 6(a); The initial penetration depth due to the cylinder weight is beyond the precision of the laser displacement measurement. Consequently, the initial penetration depth of the cylinder, $d_{i,\text{cylinder}}$, can be regarded as zero for the estimation of the penetration depth. The log-log graph in Fig. 6(b) shows the penetration depth estimation with zero for the initial penetration depth. The correlations between the penetration depth and the physical quantities are well-matched with the theories [3]. This first experiment verifies that the estimation of the penetration depth is valid in the case of the cylinder with zero for the initial penetration depth from an engineering point of view.

As the next experiment, the initial penetration depth of the ball projectile is considered. In the case of the balls, the initial penetration depths are larger than those of the cylinders as shown in the Fig. 7(a) and (b). Theoretically, the magnitude of the initial penetration depth is proportional to the square of the mass and inversely proportional to the square of the diameter (Eq. (7)). The log-log graph in Fig. 7(b) shows that the relationship between the initial penetration depth and the mass over the diameter, $d_{i,\text{ball}} \approx (m_p/D_p)^{1/2}$, is accurate for the ball projectile too (Eq. (7)). Partially due to the effect of the rotation of the ball, some variations are observed. Fig. 8 shows the predictions of the penetration depth with and without considering the buoyancy effect. As the balls are dropped with different heights, h, it is possible to obtain the experimental data with differences in the x coordinate with the same diameter. The distribution is quite consistent with the theory. These figures illustrates that there are small differences as the initial penetration depths are still small.

3.3. Experiment with cone

In order to verify the equation in Eq. (14), the experiments are carried out with cone shape projectiles. The initial penetration depth of the cone is much larger than those of cylinder and ball. Consequently, it is expected that the prediction of the penetration depth can be improved significantly with the present approach. For example, Fig. 9(a) shows the initial penetration depths of various conical projectiles. From the theory of (Eq. (12)), the initial penetration depth is proportional to one-third power of the mass and the experiment curve in Fig. 9(b) shows that the prediction is fairly accurate. Fig. 9(c) shows the curve showing the

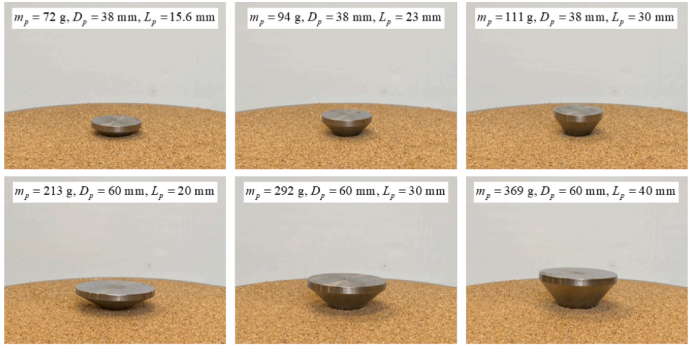

(a)

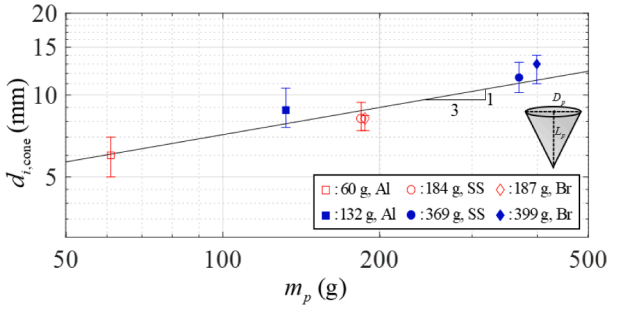

(b)

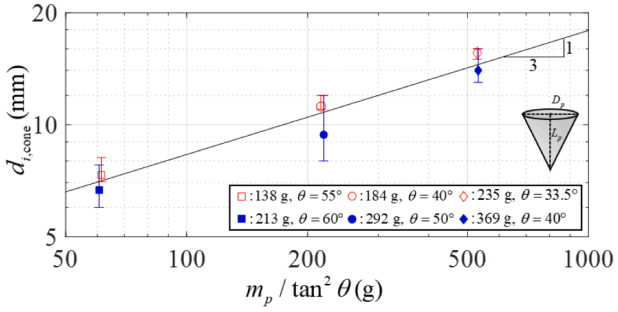

(c)

Fig. 9. Initial penetration depth experiment of cone shape projectiles. (a) The initial penetration depth distributions and (b) the experiment results of initial penetration depth distributions with respect to m_p, (i.e. $d_{i,\text{cone}} \approx m_p^{1/3}$), with the cone shape projectiles having same θ of 40° and different densities ([Red empty symbols:D_p= 48 mm, L_p= 30 mm (square: Aluminum, circle: Stainless steel, diamond: Brass)], [Blue filled symbols: D_p= 60 mm, L_p= 40 mm (square: Aluminum, circle: Stainless steel, diamond: Brass)] and (c) the experiment results of initial penetration depth distributions with respect to $m_p/\tan^2\theta$, (i.e. $d_{i,\text{cone}} \approx (m_p/\tan^2\theta)^{1/3}$), with the cone shape projectiles having different θ and the same density of aluminum ([Red empty symbols: D_p= 48 mm (square:, L_p= 20 mm, circle: L_p= 30 mm, diamond: L_p= 40 mm)], [Blue filled symbols: D_p= 60 mm (square: L_p= 20 mm, circle: L_p= 30 mm, diamond: L_p= 40 mm)]). (For interpretation of the references to colour in this figure legend, the reader is referred to the web version of this article.)

relationship between the initial penetration depth and the term, i.e. mass over $\tan^2\theta$. The theory predicts that the penetration depth is proportional to one-third power of the term and the experimental results show that this prediction is accurate, too. Note that comparing with the initial penetration depths of the cylinder projectile and the ball projectile, the initial penetration depth of the cone shape projectile is much larger and cannot be neglected. Thus, the consideration of the initial penetration depth is essential.

Fig. 10 (a) and (b) show the comparison with the estimations with and without the consideration of the initial penetration depth of cone. Without the consideration of the initial penetration depth, there are some variations on the estimation of the penetration depth in Fig. 10(a). Although the experimental results are spread, the estimation of the distribution could be possible. Our computation finds out that the power factor 1.8 could be used to correct the original prediction model (i.e. $d_{\text{cone}} = (0.09/\mu\cdot(m_p/\rho_g)^{1/2}D_p^{-5/6}H^{1/3})^{1.8}$). However, not only the equation does not match the dimension of the left and right, but the physical meaning associated with energy dissipation, which is implied by the existing formula, is undermined.

What we want to emphasize is that we do not deny that the above empirical formulation with the factor 1.8 can be employed. However, this research proposes that rather than finding the heuristic and empirical formulation for each projectile, the existing theory predicting the penetration depth of blunt projectile can be modified with the consideration of the initial penetration depth. Fig. 10(b) shows the distributions of the experimental results considering the initial penetration depth with the same data of Fig. 10(a). As shown in Fig. 10(b), the prediction becomes linear and improved. In addition, the effects of the H and m_p are independently verified in Fig. 11. As illustrated, by considering the initial penetration depth d_i, each of the parameters, the H and m_p, are well-matched with the prediction model, separately. This example explains that the penetration depth formula for blunt (or flat) projectiles can be modified by considering the initial penetration depth due to the buoyant force for sharp projectiles.

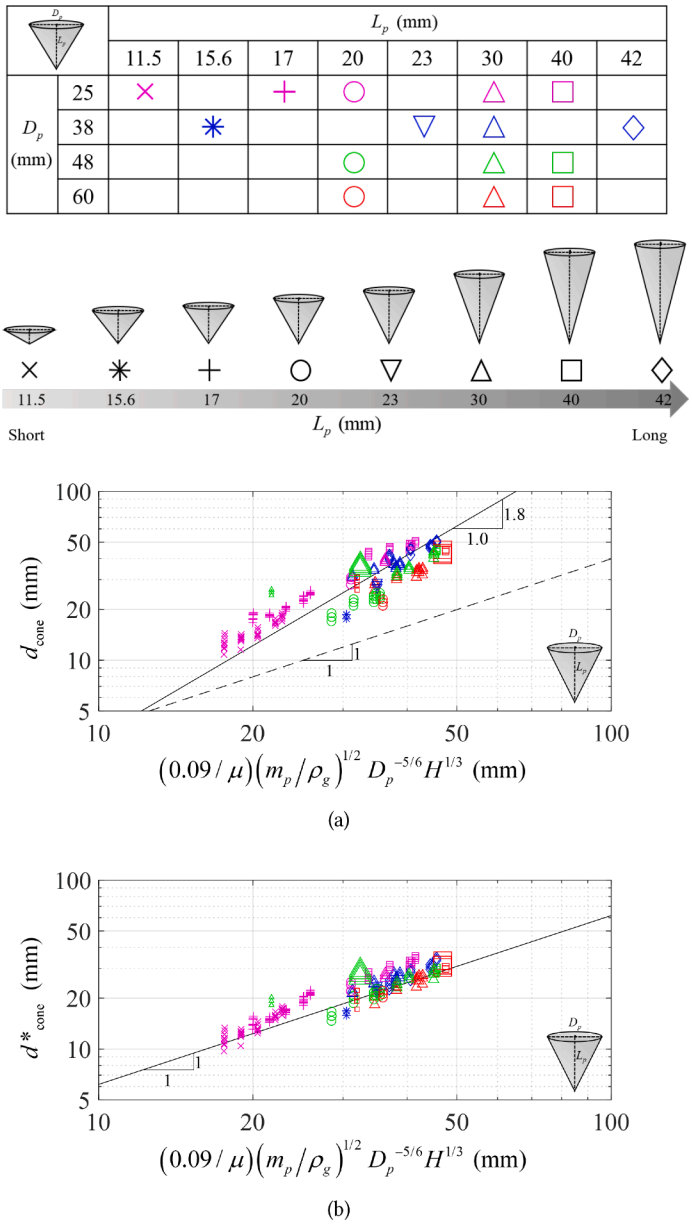

Fig. 10. Penetration depth of the cone shape projectile. (a) The penetration depth distributions without considering the initial penetration depth and (b) the modified penetration depth distributions considering the initial penetration depth ([Magenta: D_p = 25 mm (x mark: L_p=11.5 mm, plus mark: L_p=17 mm, circle: L_p=20 mm, upward-pointing triangle: L_p= 30 mm, square: L_p= 40 mm)], [Blue: D_p= 38 mm (star mark: L_p=15.6 mm, downward-pointing triangle: L_p= 23 mm, upward-pointing triangle: L_p=30 mm, diamond: L_p= 42 mm)], [Green: D_p= 48 mm (circle: L_p=20 mm, upward-pointing triangle: L_p= 30 mm, square: L_p=40 mm)], [Red: D_p= 60 mm (circle: L_p=20 mm, upward-pointing triangle: L_p=30 mm, square: L_p=40 mm)](The sizes of the symbols indicate density. From small size to big size, the symbols indicate aluminum, stainless steel and brass)). (For interpretation of the references to colour in this figure legend, the reader is referred to the web version of this article.)

4. Conclusion

This research presents a new theory considering the buoyant force to predict the penetration depth of sharp projectile. When several impactors freely fall into granular material like sand, the final penetration depths are dependent on their masses and geometries. Not to mention, their shapes also play an important role in determining the maximum penetration depth. It was found by the relevant researches that it is difficult to predict or estimate the penetration depths for sharp projectiles. In order to contribute to this research topic, several experiments with cylinder and ball were carried out. In addition, the penetration depths of cone shaped projectiles are also investigated. The investigation of the experiment data reveals that the buoyancy of projectile affects the maximum penetration depth. In addition, to consider the effect of the initial penetration depth due to the buoyant force, this research finds out that the existing formula for blunt projectiles can be modified by subtracting the initial penetration depth to the penetration depth of blunt projectiles. To prove our concept and formulation, the final penetration depths of several cone shape projectiles are presented and validated experimentally. With the present theory considering the initial depth due to the effect of the buoyant force, the final penetration depths of the three projectiles are successfully predicted and the coherence of these values is verified by the experiments. One of the limitations of the present experiment is that the compressibility of sand is not considered; Sand is whisked lightly and tapped horizontally before the experiment followed by the relevant researches. For future research topic, the effects of the compressibility, grain size, or moisture of granular material can be further investigated.

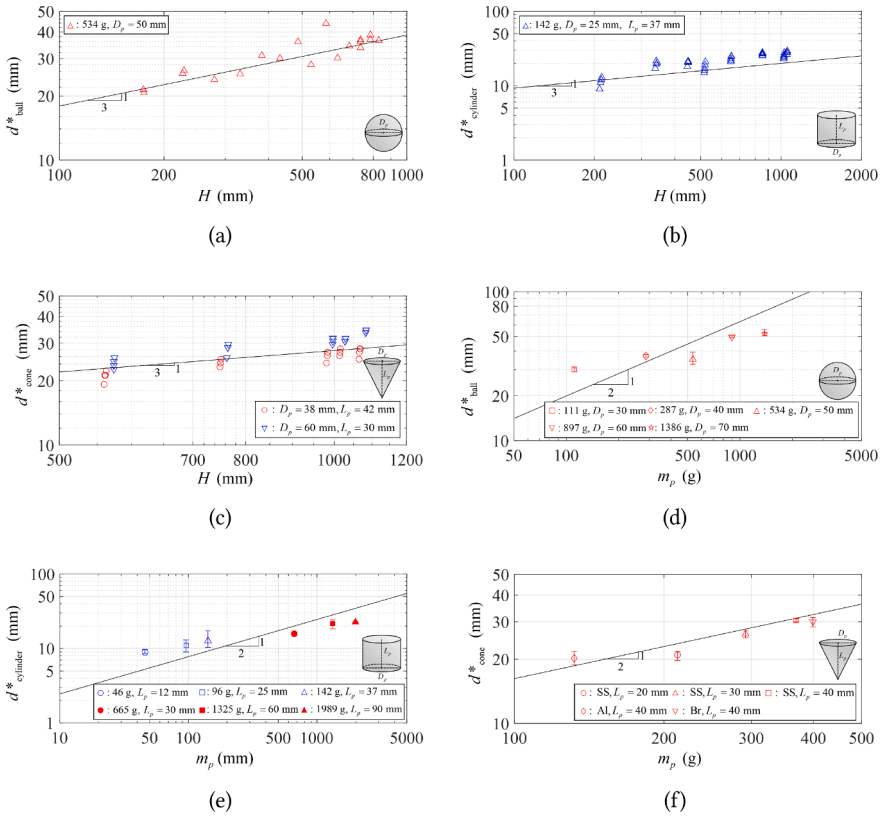

Fig. 11. The experiment results of the modified penetration depth with respect to the total drop height H of (a) ball, (b) cylinder, and (c) cone. And the experiment results of the modified penetration depth with respect to the mass of the projectiles m_p of (d) ball, (e) cylinder, and (f) cone. (For interpretation of the references to colour in this figure legend, the reader is referred to the web version of this article.)

CRediT authorship contribution statement

Hyeong Seok Koh: Conceptualization, Data curation. **Da Yeon Shin:** Conceptualization, Methodology, Writing – original draft, Writing – review & editing. **Gil Ho Yoon:** Conceptualization, Writing – original draft, Writing – review & editing.

Declaration of Competing Interest

The authors declare that they have no known competing financial interests or personal relationships that could have appeared to influence the work reported in this paper.

Acknowledgments

The authors express thank to the donor of the cadaver for the experiment and are grateful for the financial support received from the National Research Foundation (NRF) of Korea grant funded by the Korea government (MSIT) (No. 2018R1A5A7025522) and (No. 2020R1A2C2101353).

Supplementary material

Supplementary material associated with this article can be found, in the online version, at10.1016/j.ijimpeng.2022.104238.

References

[1] Uehara JS, Ambroso MA, Ojha RP, Durian DJ. Low-speed impact craters in loose granular media. Phys Rev Lett 2003;90(19):194301. https://doi.org/10.1103/PhysRevLett.90.194301.https://www.ncbi.nlm.nih.gov/pubmed/12785950
[2] Ambroso M, Santore C, Abate A, Durian DJ. Penetration depth for shallow impact cratering. Phys Rev E 2005;71(5):051305.
[3] Newhall K, Durian D. Projectile-shape dependence of impact craters in loose granular media. Phys Rev E 2003;68(6):060301.
[4] Seguin A, Bertho Y, Gondret P. Influence of confinement on granular penetration by impact. Phys Rev E 2008;78(1):010301.
[5] Ambroso M, Kamien RD, Durian DJ. Dynamics of shallow impact cratering. Phys Rev E 2005;72(4):041305.
[6] Kumar A, Khakhar D, Tripathi A. Theoretical calculation of the buoyancy force on a particle in flowing granular mixtures. Phys Rev E 2019;100(4):042909.
[7] Sandali Y, Chand R, Shi Q. "Buoyancy" in granular medium: how deep can an object sink in sand? Physica A 2016;451:560–4.
[8] Walsh AM, Holloway KE, Habdas P, de Bruyn JR. Morphology and scaling of impact craters in granular media. Phys Rev Lett 2003;91(10):104301.
[9] Lohse D, Bergmann R, Mikkelsen R, Zeilstra C, van der Meer D, Versluis M, et al. Impact on soft sand: void collapse and jet formation. Phys Rev Lett 2004;93(19):198003.
[10] Amato JC, Williams RE. Crater formation in the laboratory: an introductory experiment in error analysis. Am J Phys 1998;66(2):141–3.
[11] Loganathan TM, Sultan M, Gobalakrishnan MK, Muthaiyah G. Ballistic impact response of laminated hybrid composite materials. Mechanical and physical testing of biocomposites, fibre-reinforced composites and hybrid composites. Elsevier; 2019. p. 171–91.
[12] Bless S, Berry D, Pedersen B, Lawhorn W. Sand penetration by high-speed projectiles. AIP conference proceedings. vol. 1195. American Institute of Physics; 2009. p. 1361–4.
[13] Chian SC, Tan BCV, Sarma A. Projectile penetration into sand: relative density of sand and projectile nose shape and mass. Int J Impact Eng 2017;103:29–37.
[14] Albert I, Sample J, Morss A, Rajagopalan S, Barabási A-L, Schiffer P. Granular drag on a discrete object: shape effects on jamming. Phys Rev E 2001;64(6):061303.
[15] Collins A, Addiss J, Walley S, Promratana K, Bobaru F, Proud W, et al. The effect of rod nose shape on the internal flow fields during the ballistic penetration of sand. Int J Impact Eng 2011;38(12):951–63.
[16] Lohse D, Rauhe R, Bergmann R, Van Der Meer D. Granular physics: creating a dry variety of quicksand. Nature 2004;432(7018):689.
[17] de Bruyn JR, Walsh AM. Penetration of spheres into loose granular media. Can J Phys 2004;82(6):439–46.
[18] Pacheco-Vázquez F, Caballero-Robledo G, Solano-Altamirano J, Altshuler E, Batista-Leyva A, Ruiz-Suárez J. Infinite penetration of a projectile into a granular medium. Phys Rev Lett 2011;106(21):218001.
[19] Katsuragi H, Durian DJ. Unified force law for granular impact cratering. Nat Phys 2007;3(6):420–3.

[20] Ciamarra MP, Lara AH, Lee AT, Goldman DI, Vishik I, Swinney HL. Dynamics of drag and force distributions for projectile impact in a granular medium. Phys Rev Lett 2004;92(19):194301.
[21] Kondic L, Fang X, Losert W, O'Hern C, Behringer R. Microstructure evolution during impact on granular matter. Phys Rev E 2012;85(1):011305.
[22] Aguirre MA, Grande JG, Calvo A, Pugnaloni LA, Géminard J-C. Pressure independence of granular flow through an aperture. Phys Rev Lett 2010;104(23):238002.
[23] Brzinski III TA, Schug J, Mao K, Durian DJ. Penetration depth scaling for impact into wet granular packings. Phys Rev E 2015;91(2):022202.